Chinese Chemical Letters 37 (2026) 110979

Contents lists available at ScienceDirect

Chinese Chemical Letters

journal homepage: www.elsevier.com/locate/cclet

A NIR and ratiometric fluorescent probe for quantitative detection of SO_2 derivatives in Chinese medicinal materials and bioimaging *in vivo*

Meitong Wu[a,1], Ke Wu[a,1], Shumin Feng[a,c,*], Li Xu[a], Mi Lei[a], Jianmei Chen[a], Shuang Li[a], Mian Qin[a], Dahui Liu[a,c,*], Guoqiang Feng[b,*]

[a] School of Pharmacy, Hubei University of Chinese Medicine, Wuhan 430065, China
[b] College of Chemistry, Central China Normal University, Wuhan 430079, China
[c] Hubei Shizhen Laboratory, Hubei University of Chinese Medicine, Wuhan 430065, China

ARTICLE INFO

Article history:
Received 12 November 2024
Revised 18 February 2025
Accepted 19 February 2025
Available online 19 February 2025

Keywords:
Fluorescent probe
SO_2 derivatives metabolism
Quantitative analysis
Pinelliae rhizoma
Fluorescent imaging

ABSTRACT

Sulfur dioxide (SO_2) and its derivatives have been recognized as harmful environmental pollutants. However, they are often produced during the processing of traditional Chinese medicines, potentially compromising the quality of these medicinal materials and contributing to various health issues. Due to a lack of effective monitoring and imaging tools, the physiological effects of excessive SO_2 residues in traditional Chinese medicine remain unclear. Therefore, developing a rapid and effective tool for detecting SO_2 is crucial for understanding its metabolic pathways and effects *in vivo*. In this study, we developed a near infrared (NIR) and ratiometric fluorescent probe, **NIR-RS**, which exhibits high sensitivity, selectivity, and rapid response for SO_2 detection. Notably, **NIR-RS** accurately quantifies SO_2 contents in *Pinelliae rhizoma* (*P. rhizoma*) samples, with recovery rates from 98.46 % to 102.40 %, and relative standard deviations (RSDs) $<$ 5.0 %. For bioimaging applications, **NIR-RS** has low cytotoxicity and good mitochondrial-targeting ability, making it suitable for imaging exogenous and endogenous SO_2 in mitochondria. Additionally, **NIR-RS** was successfully applied to image SO_2 content of *P. rhizoma* samples within cells, revealing that high SO_2 residue elevated mitochondria adenosine triphosphate (ATP) content, these findings reveal that *P. rhizoma* with excessive SO_2 can affect the organism's growth mechanisms through alterations in ATP pathways. *In vivo*, SO_2 was found to predominantly accumulate in the liver following gavage with *P. rhizoma* solution, with accumulation levels increasing in proportion to SO_2 residue concentration. High SO_2 concentrations in *P. rhizoma* can cause pulmonary fibrosis and gastric mucosal damage. This work provides a valuable tool for regulating SO_2 content in *P. rhizoma* and may help researcher better understand the metabolism of SO_2 derivatives and explore their physiological roles in biological systems.

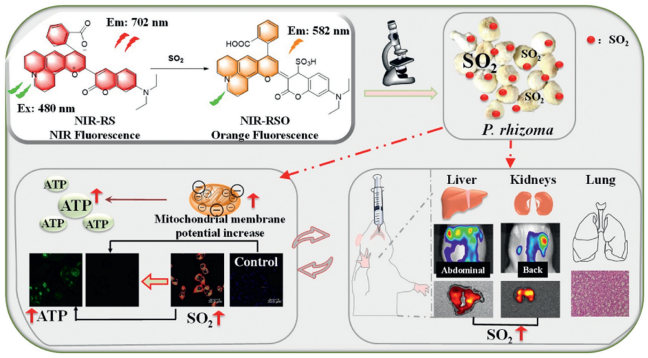
© 2025 Published by Elsevier B.V. on behalf of Chinese Chemical Society and Institute of Materia Medica, Chinese Academy of Medical Sciences.

Sulfur dioxide (SO_2) is both a main atmospheric pollutant and a valuable commercial reagent, it is often produced through the combustion of sulfur-containing raw materials and fuels [1]. It can dissolve in water and form a pH-dependent equilibrium between sulfite (SO_3^{2-}) and bisulfite (HSO_3^-) with a 1:3 molar ratio [2,3]. In the industry, sulfur processing (including sulfur fumigation, pyrosulfite soaking, *etc.*) is widely used to protect food, beverages, and Chinese medicinal materials from spoilage due to its antioxidant and enzyme inhibition properties [4–6]. For instance, *Pinelliae rhizoma* (*P. rhizoma*) is usually processed with fumigation or sodium pyrosulfite to ensure long-term storage and maintain good color [7,8]. However, a large amount of SO_2 usually remains in *P. rhizoma* after treatment, which will reduce the medicinal ingredients of *P. rhizoma* [9], and the toxicological studies unveil that SO_2 is associated with lung cancer, cardiovascular diseases [10], and neurological diseases [11] may involve the formation of sulfur-and oxygen-centered free radicals that disturb the molecular mechanism of mitochondrial and affect cell physiological activity [12]. Hence, the residual of SO_2 in Chinese medicinal materials is strictly controlled, and the amount of SO_2 should be $<$150 mg/kg according to Pharmacopoeia of People's Republic of China [13]. Hence, developing a fast and efficient way for monitoring SO_2 residue in real Chinese herbal medicine is imperative.

Several methods for detecting SO_2 have been reported, including acid-base titration [14], gas chromatography [15], ion chromatography [16], and fluorescence analysis [17]. Among these methods, fluorescence analysis stands out for its simple opera-

* Corresponding authors.
E-mail addresses: fsm3318@hbucm.edu.cn (S. Feng), liudahui@hbucm.edu.cn (D. Liu), gf256@mail.ccnu.edu.cn (G. Feng).
[1] These authors contributed equally to this work.

https://doi.org/10.1016/j.cclet.2025.110979
1001-8417/© 2025 Published by Elsevier B.V. on behalf of Chinese Chemical Society and Institute of Materia Medica, Chinese Academy of Medical Sciences.



Scheme 1. The sensing mechanism of the probe **NIR-RS** to detect SO_2 and the simple diagram of **NIR-RS** imaging SO_2 in cell and *in vivo*.

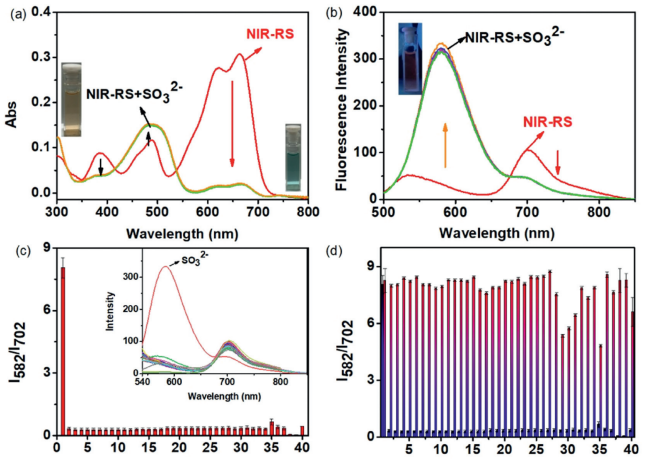


Fig. 1. (a) Ultraviolet (UV) spectrum changes of **NIR-RS** (10 μmol/L) in the presence of SO_2 derivative (200 μmol/L). (b) Fluorescence spectrum changes of **NIR-RS** (10 μmol/L) detection of SO_2 derivative (200 μmol/L). (c) Fluorescence ratio (I_{582}/I_{702}) of **NIR-RS** upon addition of various analytes (200 μmol/L). 1–40: HSO_3^-, blank, Cl^-, I^-, HCO_3^-, OCN^-, AcO^-, $C_2O_4^{2-}$, $S_2O_7^{2-}$, HSO_4^-, F^-, Br^-, SCN^-, NO_2, $S_2O_3^{2-}$, Ser, Glu, Lys, Arg, Gly, Phe, His, Ala, Met, Ile, Gln, Thr, Ca^{2+}, Zn^{2+}, Al^{3+}, Fe^{3+}, Cu^{2+}, Mg^{2+}, 5 mmol/L GSH, 200 μmol/L NaHS, Hcy, Cys, S_8, CH_3SSSCH_3, Na_2S_2 (insert fluorescence spectrum). (d) Competition experiments of **NIR-RS** for the above various analytes. All experiments were performed in PBS buffer (10 mmol/L, pH 7.4) with 30 % DMF at 37 °C. λ_{ex} = 480 nm, slit width (10, 10). Data are presented as mean ± standard deviation (SD) (n = 3).

tion, and high sensitivity [18], especially the ratiometric and near-infrared (NIR) fluorescence, which has a lot of advantages: high accuracy, low autofluorescence interference, deep tissue penetration [19,20], rendering it ideal for quantitative detecting SO_2 residues in Chinese herbal medicine, and tracking effect of the SO_2 residues *in vivo* [21].

Herein, a mitochondrial-targeted fluorescent probe (**NIR-RS** in Scheme 1), that can be used for colorimetric and ratiometric detecting SO_2 in *P. rhizoma* and *in vivo* was developed. The coumarin-semirhodamine hybrid structure of probe **NIR-RS**, features near-infrared fluorescence, excellent water solubility, and high quantum yield [22,23]. Upon addition of SO_2, probe **NIR-RS** displays a distinct colorimetric and ratiometric fluorescence change in the far-red and NIR region (λ_{em} = 582 and 702 nm), and exhibited high sensitivity (Limit of detection (LOD) = 50 nmol/L), excellent selectivity. Importantly, probe **NIR-RS** can accurately detect SO_2 content in *P. rhizoma* samples, the recovery rates from 98.46 % to 102.40 %, with relative standard deviations (RSDs) < 5.0 %. Moreover, **NIR-RS** was successfully used to image both endogenous and exogenous SO_2 in mitochondria. Using **NIR-RS** and **Rho-ATP** (a probe for detecting adenosine triphosphate (ATP)) [24] for optical imaging, we found that high SO_2 residue in *P. rhizoma* increased ATP levels in mitochondria. This is the first fluorescent probe to evaluate the link between the high SO_2 residue of *P. rhizoma* and ATP expression in cells. Additionally, when mice were orally administered *P. rhizoma* with high SO_2 residue, SO_2 mainly accumulates in the liver, and can also cause pulmonary fibrosis and gastric mucosal damage. In summary, we developed a standardized tool for measuring SO_2 residue in *P. rhizoma* and provided a new method for studying the metabolic effects of high SO_2 residue *in vivo*.

First, compounds **1** and **2** were prepared by a literature method [25,26], and the synthesis of probe **NIR-RS** is outlined in Scheme S2 (Supporting information). Compounds **1** and **2** in methylsulfonic acid at 120 °C to afford **NIR-RS** in 23 % yield. The structure of **NIR-RS** was confirmed by nuclear magnetic resonance (NMR) and mass spectroscopy (Figs. S1–S4 in Supporting information).

Next, the performance of **NIR-RS** for detecting SO_2 was studied in phosphate buffered solution (PBS) (10 mmol/L, pH 7.4, 30 % dimethylformamide (DMF), v/v) by measuring the absorption and fluorescence changes. As expected, **NIR-RS** has large conjugated structures and shows an absorption maxima at 660 nm and a fluorescence peak at 702 nm in the test solution (Fig. 1). However, the maximum absorption peak of **NIR-RS** at 660 nm was decreased abruptly when 200 μmol/L HSO_3^- was added, and the absorption peak at 480 nm emerged, together with an obvious color change from green to pale pink (Fig. 1a). This indicates that **NIR-RS** can be used as a colorimetric probe for HSO_3^-. Meanwhile, after HSO_3^- was added, the fluorescence of **NIR-RS** decreased significantly at 702 nm and concurrently increased at 582 nm (Fig. 1b), the results indicate that **NIR-RS** is a good ratiometric fluorescent probe for SO_3^{2-}. We also monitored the fluorescence intensity changes of **NIR-RS** (10 μmol/L) at 582 and 702 nm after adding HSO_3^-, HS^-, glutathione (GSH), homocysteine (Hcy), and cysteine (Cys), respectively, and kinetics results showed a fast reaction rate (<1 min, Fig. S6 in Supporting information) upon add SO_3^{2-}, and negligible changes were observed upon the addition of biothiol (HS^-, GSH, Hcy and Cys). Then, we investigated the response of **NIR-RS** to various biologically relevant analytes, including Cl^-, I^-, HCO_3^-, OCN^-, AcO^-, $C_2O_4^{2-}$, $S_2O_7^{2-}$, HSO_4^-, F^-, Br^-, SCN^-, NO_2^-, $S_2O_3^{2-}$, Ser, Glu, Lys, Arg, Gly, Phe, His, Ala, Met, Ile, Gln, Thr, Ca^{2+}, Zn^{2+}, Al^{3+}, Fe^{3+}, Cu^{2+}, Mg^{2+}), S_8, Na_2S_2, CH_3SSSCH_3. It was found only HSO_3^- can cause a significant fluorescence change, this indicates that **NIR-RS** is high selectivity for HSO_3^- over other analytes (Fig. 1c). Meanwhile, the competition experiments showed that all these biologically relevant analytes displayed almost no interference with HSO_3^- detection (Fig. 1d). What is more, **NIR-RS** exhibited excellent photostability under 365 nm light exposure for 120 min (Fig. S7 in Supporting information). These illustrated that **NIR-RS** displayed remarkable selectivity to HSO_3^- detection. Then, we sought to investigate the pH effect on the fluorescence behavior of **NIR-RS** in the detection of HSO_3^-, As shown in Fig. S8 (Supporting information), the ratio of fluorescence intensities of **NIR-RS** did not show significant changes, representing that this probe was stable in a wide range of pH. Notably, once HSO_3^- was added to the **NIR-RS** solution, the ratio of fluorescence intensities (I_{582}/I_{702}) was increased in the solution of **NIR-RS** with SO_3^{2-} in the pH range of 6–11. This pH range for **NIR-RS** in the detection of HSO_3^- implied its potential application in environmental and biological studies.

After confirming the high selectivity of **NIR-RS** for HSO_3^-, then the sensitivity of **NIR-RS** to SO_3^{2-} was investigated. As shown in Fig. 2a, with increased concentrations of HSO_3^-, the fluorescence of **NIR-RS** decreased gradually at 702 nm while increasing obviously at 582 nm. The fluorescence intensities at 582 nm continued to rise and saturated after the addition of about 300 μmol/L of SO_2 derivative. A linear relationship (R^2 = 0.99333) was observed between the fluorescence intensity ratio (I_{582}/I_{702}) and HSO_3^- concentration over the range of 0–200 μmol/L (Fig. 2b). The detection

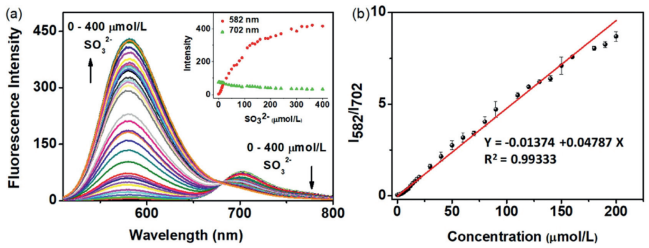


Fig. 2. Fluorescent spectral changes of probe **NIR-RS** (10 μmol/L) upon addition of HSO_3^- (0–400 μmol/L) Insert: Fluorescence intensity changes at 582 and 702 nm. (b) The linear relationship between the variation in fluorescence ratio (I_{587}/I_{702}) and HSO_3^- in the range of 0–200 μmol/L. λ_{ex} = 480 nm, slit width (10, 10). Data are presented as mean ± SD (n = 3).

limit was calculated to be 50 nmol/L, based on signal to noise ratio (S/N) = 3, indicating that **NIR-RS** can be effectively employed for quantitative detection of HSO_3^- over a broad linear range. These results suggest that **NIR-RS** has a high sensitivity to HSO_3^- and is suitable for detecting SO_2 derivatives in Chinese herbal medicine samples.

To investigate the application properties of **NIR-RS**, we evaluated its effectiveness in determining SO_2 content in *P. rhizoma* samples. First, *P. rhizoma* samples treated with different concentrations of sodium pyrosulfite were measured by **NIR-RS.** As shown in Table S1 (Supporting information), the probe successfully detected SO_2 content in the samples, with a relative standard deviation RSD of <5 %. Furthermore, the results obtained from this method closely aligned with those from the national standard titration method (Table S2 in Supporting information) [14]. *T*-test analysis revealed no statistically significant difference between the two methods (P > 0.05), and the recovery rates of **NIR-RS** detecting SO_2 in *P. rhizoma* samples ranged from 98.46 % to 102.40 % (Table S3 in Supporting information). These results demonstrate that **NIR-RS** is suitable for accurately and precisely detecting SO_2 content in *P. rhizoma* samples. To our knowledge, few fluorescent probes are capable of detecting SO_2 in Chinese herbal medicine samples, which is likely attributable to the ratiometric property of **NIR-RS** that enhances detection precision.

To understand the sensing mechanism of **NIR-RS** for HSO_3^-, considering the optical sign at 582 nm of **NIR-RS** for detecting HSO_3^- was increased, suggesting that **NIR-RSO** showed the fluorescence of semi-rhodamine while **NIR-RS** was taken addition with HSO_3^- at the site 4 of coumarin, and the conjugated skeleton of **NIR-RS** was interrupted and generated compound **NIR-RSO**. To prove this, HPLC-MS analysis was carried out, and a mass peak at *m/z* 561.2391 corresponded to the addition adduct of N**IR-RS**, in addition, the peak that appeared at *m/z* 641.1967 was attributed to compound **NIR-RSO** (Fig. S9 in Supporting information). Thus, based on the reports of several recently reported semirhodamine-based HSO_3^- probes [27–29], the sensing mechanism of probe **NIR-RS** for HSO_3^- was proposed as a process as shown in Scheme S2.

Before imaging, the MTT assays were used to evaluate the cytotoxicity of **NIR-RS**, as shown in Fig. S10 (Supporting information), **NIR-RS** exhibits no significant cytotoxicity. Mitochondria play essential roles in energy metabolism, and the SO_2 derivate was linked with mitochondrial disturbances [30,31]. The cationic probe **NIR-RS** can easily bind to the mitochondrial membrane with a negative potential (−250 mV) [32], which may accumulate in mitochondria. Then, the colocalization imaging experiment was performed to evaluate the distribution of **NIR-RS** (Fig. S11 in Supporting information). When the **NIR-RS** and a commercialized Mito-Tracker Green (**MTG**) were co-incubated in cells the cytoplasm merged image showed the fluorescence distribution in green and red channels overlapped well, and the intensity profiles of the linear regions of interest (ROI) across the cells also displayed an excellent correlation. To further understand the distribution of the probe **NIR-RS** in the cells, other commercial dyes, including Hoechst 33342 (nucleus), LysoTracker Green (lysosomes), Golgi-Tracker Green (Golgi), ER-Tracker Green (endoplasmic reticulum) was also incubated with probe **NIR-RS**, as shown in Fig. S12 (Supporting information), we found that Pearson's co-localization was higher in mitochondria then other subcellular organelles. Additionally, the Pearson's co-localization and overlap coefficients in mitochondria were calculated to be 0.87 and 0.90, respectively. The above results indicated that **NIR-RS** possesses a mitochondria-targeting capability with low cytotoxicity, and has the potential ability to track and image SO_2 in mitochondria.

Cell imaging experiments were carried out to study the imaging performance of the probe **NIR-RS** for detecting SO_2. First, HeLa cells were incubated with **NIR-RS** for 30 min, and strong red fluorescence and weak green fluorescence were observed, indicating that **NIR-RS** has great cell membrane permeability (Fig. S13 in Supporting information). However, when the cells were incubated with different concentrations of exogenous SO_2 (HSO_3^-), a remarkable increase in the green channel and a reduction in red fluorescence was observed (Figs. S13b and c). These results manifested that **NIR-RS** could effectively detect exogenous SO_2. In addition, when cells were preincubated with Cys to produce endogenous SO_2 [33], the fluorescence ratio of I_{green}/I_{red} increased (Fig. S14 in Supporting information), and decreased in the presence of tetrahydrofolate (an endogenous formaldehyde (FA) reagent), this suggests that **NIR-RS** has the potential to detect endogenous SO_2. Overall, these experiments show that **NIR-RS** is suitable for imaging both exogenously and endogenously SO_2 in cells.

We further investigated the property of **NIR-RS** to image SO_2 residual in *P. rhizoma* sample within cells. As shown in Fig. 3, when cells were incubated with *P. rhizoma* sample containing different concentrations of SO_2, a dramatical increase in the green-to-red fluorescence ratio was observed, with a pronounced enhancement in the green channel and a decline in red channel fluorescence as SO_2 levels increased (Fig. 3a). However, when FA was co-incubated with 5 g/kg *P. rhizoma* sample, the red fluorescence was restored, and the green/red fluorescence ratio was depressed. These results indicated that *P. rhizoma* fumigated with high sodium pyrosulfite content leads to elevated SO_2 expression in cells. Elevated SO_2 levels were found to increase the inner mitochondrial membrane potential (Fig. 3b), which is reported to reflect an energized mitochondrion with enhanced ATP production capacity [34]. Using **Rho-ATP** (Fig. 3c), we measured mitochondrial function by assessing ATP production (Fig. 3d). Cells incubated with 5 mg/kg *P. rhizoma* displayed an increase in green fluorescence, while cells treated with apyrase (a hydrolytic enzyme that can convert ATP into adenosine monophosphate (AMP) and inorganic phosphate) [35–37] showed weak green fluorescence. This indicates that SO_2-induced mitochondrial ATP production surged, potentially disturbing intracellular energy metabolism and impairing normal cellular function. Then, HeLa cells were pre-incubated with different concentrations of SO_2 residual from *P. rhizoma* samples. Cells incubated with *P. rhizoma* (1, 3, 5 g/kg) displayed an increase in green fluorescence compared to the blank group. The fluorescence intensity generally increased with higher SO_2 concentrations and reached a peak at 3 g/kg (Fig. S15 in Supporting information). These findings reveal that *P. rhizoma* with excessive SO_2 can affect the organism's growth mechanisms through alterations in ATP pathways. This provides a new direction for researchers to explore the physiological effects of *P. rhizoma* with excessive SO_2 residues *in vivo*.

Encouraged by the outcomes of the cellular experiments, we scrutinized the potential of **NIR-RS** to image SO_2 *in vivo*. Kunming

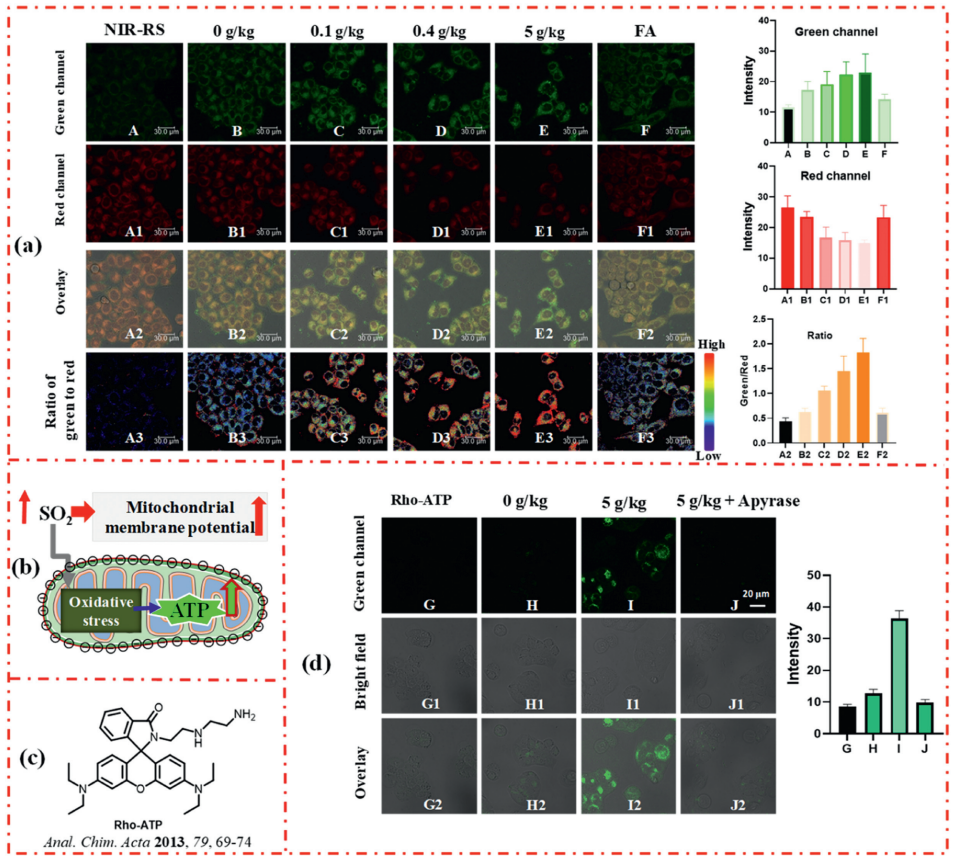


Fig. 3. Imaging the changes of different concentrations of SO_2 residual in *P. rhizoma* sample within cells. (a) The HeLa cells were incubated with 10 μL *P. rhizoma* sample solution 0 g/kg (B), 0.1 g/kg (C), 0.4 g/kg (D), 5 g/kg (E), then treated with 5 μmol/L NIR-RS for 30 min. (F) The HeLa cells were incubated with 10 μL *P. rhizoma* (5 g/kg) solution and 200 μmol/L HCHO, then treated with 5 μmol/L **NIR-RS** for 30 min. The green channel (Em = 540–590 nm, with λ_{ex} = 488 nm), and the red channel (Em = 680–720 nm, with λ_{ex} = 633 nm). Scale bar: 30 μm. (b) The simple diagram of mitochondrial ATP change under SO_2 stimulation. (c) The structure of Probe **Rho-ATP**. (d) Imaging the ATP concentration changes of high SO_2 residual in *P. rhizoma* sample within cells. Scale bar: 20 μm. The HeLa cells were incubated with 10 μmol/L **Rho-ATP** for 20 min (G). The HeLa cells were incubated with *P. rhizoma* samples 0 g/kg (H), 5 g/kg (I) for 30 min, then incubated with 10 μmol/L **Rho-ATP** for 20 min; The HeLa cells were incubated with *P. rhizoma* samples (5 g/kg) and 1 UN/mL apyrase for 30 min, then incubated with 10 μmol/L **Rho-ATP** for 20 min (J). Quantification of fluorescence intensity of green channel (E_m = 570–620 nm, with λ_{ex} = 561 nm). Data are presented as mean ± SD (n = 3).

mice were purchased from the Hubei Provincial Center for Disease Control and Prevention (Wuhan, China). All the animal experiment procedures were approved by the Animal Experiment Center of Hubei University of Chinese Medicine and followed the Guidelines for the Care and Use of Research Animals. As shown in Fig. S16 (Supporting information), when the mouse was intravenously injected with **NIR-RS**, a strong fluorescence signal at 710 nm was observed. Upon orthotopic injection of SO_3^{2-}, the 710 nm signal rapidly diminished, accompanied by a significant fluorescence increase at 570 nm within 1 min, indicating that **NIR-RS** can rapidly track SO_3^{2-} *in vivo*. Then, we further investigated the property of **NIR-RS** to image SO_2 residual from *P. rhizoma* sample *in vivo*. As shown in Fig. S17 (Supporting information), the 0 g/kg *P. rhizoma* group showed a stronger sign in the red channel. As the sodium pyrosulfite content in *P. rhizoma* increased, the fluorescence in the red channel decreased, while the green channel signal intensified. The results indicated that the **NIR-RS** could effectively detect SO_2 residues in *P. rhizoma* samples *in vivo*.

To investigate the actual effects of excessive sulfur dioxide in the *P. rhizoma* sample on organisms, Kunming mice were orally gavaged with 0.5 mL *P. rhizoma* sample (0, 0.4, 5 g/kg) for 8 consecutive days. Histological analysis indicated the mice treated with *P. rhizoma* sample (5 g/kg) exhibited signs of pulmonary fibrosis and gastric mucosal damage (Fig. S18 in Supporting information), while other tissues were minimally affected. In addition, tissue damage assessment experiments showed that the probe **NIR-RS** was relatively safe at (100 μmol/L, in 100 μL PBS buffer solution) doses (Fig. S19 in Supporting information). Notably, as shown in Figs. 4a–d, SO_2 residues were detected *in vivo*. In the 0 and 0.4 g/kg groups, distinct fluorescent signals were observed in the liver and kidneys at the 710 nm channel. Compared to the other two groups, the 0.4 g/kg group displayed significantly stronger fluorescence intensity (Fig. 4f). This suggests that mice administered 0.4 g/kg *P. rhizoma* sample may have reduced liver metabolic efficiency, leading to the accumulation of **NIR-RS** in the liver. The ratiometric properties of the **NIR-RS** probe indicated that SO_2 residue concentrations increased, and the SO_2 levels in the liver and kidneys also rose (Figs. 4e and f), indicating that SO_2 tends to accumulate in these organs. Additionally, the imaging confirmed the presence of excessive SO_2 residues in liver and kidney tissues (Fig. S20 in Supporting information), providing insights into the metabolic pathways for *P. rhizoma* samples containing SO_2 residues.

In summary, we designed a fluorescent probe **NIR-RS** for detecting SO_2 residues in *P. rhizoma* samples and living systems. Probe **NIR-RS** exhibits high sensitivity (LOD = 50 nmol/L), selectivity, and a rapid response for SO_2 detection. It was successfully used for quantitative analysis of SO_2 residues, with recovery rates ranging from 98.46 % to 102.40 % and RSDs < 5.0 %. In addition, **NIR-RS** has low cytotoxicity and good mitochondrial-targeting ability to image both mitochondrial exogenous and endogenous SO_2. Importantly, we found that *P. rhizoma* with high SO_2 residues increases ATP levels in mitochondria, Probe **NIR-RS** imaging *in vivo* demon-

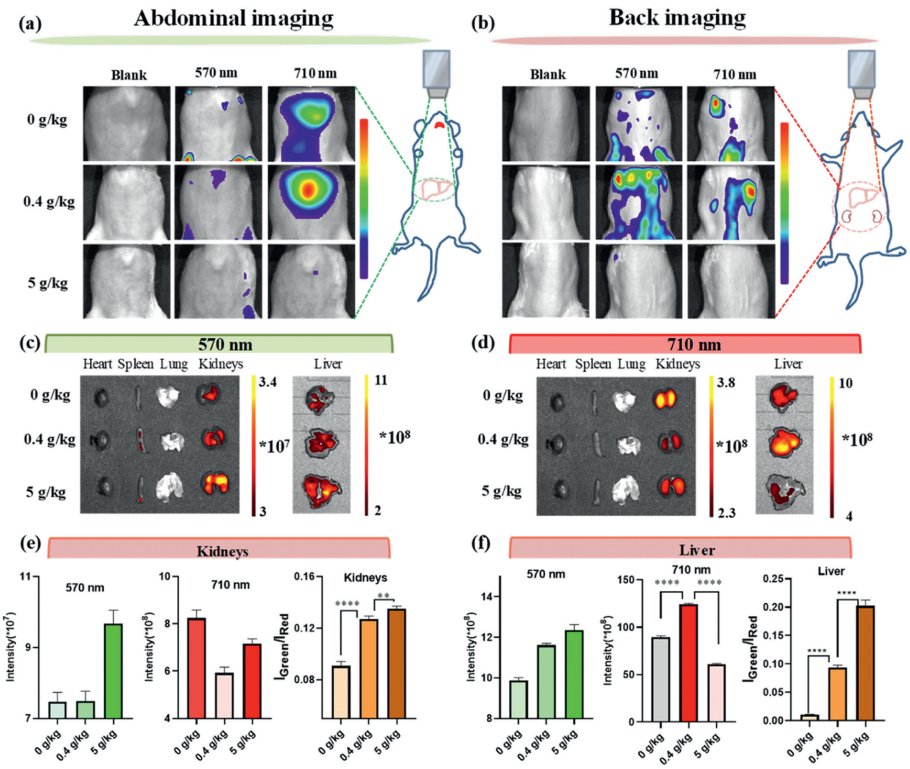


Fig. 4. Fluorescence imaging of the mice (0, 0.4, 5 g/kg groups) after intravenous injection of **NIR-RS** (100 μL, 100 μmol/L). (a) Mice abdominal imaging. (b) Mice back imaging. Fluorescence imaging at 570 nm (c) and 710 nm (d) of the heart, liver, spleen, lung, and kidneys after 10 min of tail vein injection of **NIR-RS**. (e) Plot of the intensity of images kidneys. (f) Plot of the intensity of images liver. Fluorescence quantification analysis of the liver at 570 and 710 nm. Data are represented as the mean ± SD ($n = 4$). $^{**}P < 0.01$, $^{****}P < 0.0001$.

strated its excellent ability to monitor SO_2 residue metabolism, and excessive intake of *P. rhizoma* containing high SO_2 residue can cause pulmonary fibrosis and gastric mucosal damage. Overall, this study provides a powerful tool for regulating SO_2 residue levels in *P. rhizoma* and offers new methods for tracking SO_2 metabolism *in vivo*. It also opens new avenues for researching the pathological and physiological toxicity of SO_2 residues in *P. rhizoma*.

Declaration of competing interest

The authors declare that they have no known competing financial interests or personal relationships that could have appeared to influence the work reported in this paper.

CRediT authorship contribution statement

Meitong Wu: Writing – original draft, Methodology, Investigation, Data curation, Conceptualization. **Ke Wu:** Investigation, Formal analysis, Data curation, Conceptualization. **Shumin Feng:** Writing – review & editing, Writing – original draft, Supervision, Project administration, Conceptualization. **Li Xu:** Methodology, Investigation, Formal analysis, Data curation. **Mi Lei:** Methodology, Formal analysis, Data curation. **Jianmei Chen:** Methodology, Investigation. **Shuang Li:** Methodology, Investigation. **Mian Qin:** Methodology, Investigation. **Dahui Liu:** Writing – review & editing, Supervision, Project administration, Funding acquisition. **Guoqiang Feng:** Writing – review & editing, Supervision, Project administration.

Acknowledgments

This work was supported by the Natural Science Foundation of Hubei Province (Nos. 2023AFB376 and 2024AFD287), National Key Research and Development Program (No. 2023YFC3503804) and the National Natural Science Foundation of China (No. 22077044).

Supplementary materials

Supplementary material associated with this article can be found, in the online version, at doi:10.1016/j.cclet.2025.110979.

References

[1] J. Xu, H. Yuan, G. Bao, et al., Chin. Chem. Lett. 29 (2018) 1456–1464.
[2] F. Li, L. Zou, X. Duan, et al., J. Photochem. Photobiol. A: Chem. 411 (2021) 113201.
[3] Y. Yang, X. Yan, K. Zhong, et al., J. Hazard. Mater. 469 (2024) 134003.
[4] X. Jiang, L. Huang, S. Chen, et al., Phytomedicine 20 (2013) 97–105.
[5] J. Zhao, C. Zheng, W. Zhu, et al., Chem. Biol. Interact. 292 (2018) 84–93.
[6] S. Zhou, J. Hu, S. Li, et al., J. Hazard. Mater. 364 (2019) 376–387.
[7] X. Han, H. Zheng, F. Wang, et al., Spectrochim. Acta A: Mol. Biomol. Spectrosc. 317 (2024) 124463.
[8] J. Bai, J. Qi, Y. Shi, et al., J. Ethnopharmacol. 298 (2022) 115650.
[9] Z. Zhan, A. Deng, L. Huang, et al., J. Pharm. Biomed. Anal. 156 (2018) 340–348.
[10] L. Zhang, L. Zhang, L. Chen, et al., TrAC Trends Anal. Chem. 169 (2023) 117377.
[11] L. Zou, J. Xu, X. Duan, et al., Microchem. J. 153 (2020) 104461.
[12] N. Sang, Y. Yun, G. Li, et al., Toxicol. Sci. 114 (2010) 226–236.
[13] Chinese Pharmacopoeia Commission, Pharmacopoeia of the People's Republic of China (Volume 4: Other General Rules), The Medicine Science and Technology Press of China, Beijing, 2020, pp. 29–34.
[14] A. Nieto-Márquez, E. Atanes J. Valverde, et al., Fuel. Process. Technol. 144 (2016) 274–281.
[15] H. Wang, L. Zhou, J. Sun, et al., Int. J. Hydrog. Energ. 35 (2010) 2994–2996.
[16] X. Yao, C. Lee, C. Whitelaw, et al., Atmos. Environ. 45 (2011) 2781–2788.
[17] K. Dou, Q. Fu, J. You, et al., Biomaterials 133 (2017) 82–93.
[18] H. Jin M. Yang, R. Gui, et al., Coord. Chem. Rev. 446 (2021) 214114.
[19] L. Wu, A. Sedgwick, T. James, et al., Acc. Chem. Res. 52 (2019) 2582–2597.
[20] Q. Fu, X. Yang, J. Song, et al., ACS Nano 18 (2024) 3916–3968.
[21] F. Yan, J. Cui, C. Wang, et al., Chin. Chem. Lett. 33 (2022) 4219–4222.
[22] D. Cheng, L. Yuan, X. Zhang, et al., Anal. Chem. 92 (2020) 11396–11404.
[23] Y.T. Yang, H. Zhong, B.H. Wang, et al., Chin. Chem. Lett. 34 (2023) 107674.
[24] C. Li, C. Zou, W. Zhu, et al., Anal. Chim. Acta 795 (2013) 69–74.

[25] Q. Xia, S. Feng, G. Feng, et al., Sens. Actuat. B: Chem. 337 (2021) 129732.
[26] S. Feng, D. Liu, G. Feng, Anal. Chim. Acta 1054 (2019) 137–144.
[27] L. Wang, L. Zhao, H. Liu, et al., Microchem. J. 160 (2021) 105703.
[28] X. Bao, X. Cao, C. Huo, et al., J. Agric Food Chem. 69 (2021) 4903–4910.
[29] M. Hou, Z. Wang, C. Li, et al., Talanta 265 (2023) 124815.
[30] G. Qin, M. Wu, N. Sang, et al., Toxicol. Sci. 151 (2016) 334-246.
[31] G. Qin, J. Wang, N. Sang, et al., Toxicology 300 (2012) 67–74.
[32] L. Huang, Y. Zhou, X. Xue, et al., Aggregate 5 (2023) e403.
[33] J. Yin, Y. Ma, W. Lin, et al., Coord. Chem. Rev. 412 (2020) 213257.
[34] N. Iwase, T. Sasaki, K. Shirato, et al., J. Clin. Invest. 99 (1997) 1651–1661.
[35] U. Tamima, S. Sarkar, K. Ahn, et al., Angew. Chem. Int. Ed. 62 (2023) e202300580.
[36] B. Yang, R. Tian, Z. Wang, et al., Anal. Chem. 95 (2023) 5034–5044.
[37] J. Chen, S. Chen, C. Li, et al., Anal. Chem. 95 (2023) 2119–2127.